Water-Sensitive Low-Frequency Vibrations of Reaction Intermediates during S-State Cycling in Photosynthetic Water Oxidation†

Yukihiro Kimura,*,‡ Asako Ishii,‡ Toshihiro Yamanari,§ and Taka-aki Ono*,‡

Laboratory for Photo-Biology (1), RIKEN Photodynamics Research Center, Institute of Physical and Chemical Research, 519-1399 Aoba, Aramaki, Aoba, Sendai 980-0845, Japan, and Faculty of Integrated Arts and Sciences, Hiroshima University, 1-7-1 Kagamiyama, Higashi-Hiroshima 739-8521, Japan

Received August 19, 2004; Revised Manuscript Received February 17, 2005

ABSTRACT: In photosynthetic water oxidation, two water molecules are converted to an oxygen molecule through five reaction intermediates, designated S_n ($n = 0-4$), at the catalytic Mn cluster of photosystem II. To understand the mechanism of water oxidation, changes in the chemical nature of the substrate water as well as the Mn cluster need to be defined during S-state cycling. Here, we report for the first time a complete set of Fourier transform infrared difference spectra during S-state cycling in the low-frequency (670−350 cm^{-1}) region, in which interactions between the Mn cluster and its ligands can be detected directly, in PS II core particles from *Thermosynechococcus elongatus*. Furthermore, vibrations from oxygen and/or hydrogen derived from the substrate water and changes in them during S-state cycling were identified using multiplex isotope-labeled water, including $H_2{}^{18}O$, $D_2{}^{16}O$, and $D_2{}^{18}O$. Each water isotope affected the low-frequency S-state cycling spectra, characteristically. The bands sensitive only to $^{16}O/^{18}O$ exchange were assigned to the modes from structures involving Mn and oxygen having no interactions with hydrogen, while the bands sensitive only to H/D exchange were assigned to modes from amino acid side chains and/or polypeptide backbones that associate with water hydrogen. The bands sensitive to both $^{16}O/^{18}O$ and H/D exchanges were attributed to the structure involving Mn and oxygen structurally coupled with hydrogen in a direct or an indirect manner through hydrogen bonds. These bands include the changes of intermediate species derived from substrate water during the process of photosynthetic water oxidation.

Photosynthetic water oxidation occurs in an oxygen-evolving complex (OEC),[1] in which the catalytic center comprises a tetranuclear Mn cluster and associated Ca and Cl ions, residing on the lumenal side of photosystem (PS) II. Two water molecules are oxidized to an oxygen molecule by the OEC through a light-driven process, in which the OEC changes in a stepwise manner from the lowest oxidized S_0 state to the highest oxidized S_4 state by an oxidizing equivalent generated at the PS II reaction center by absorption of a photon. The S_1 state is thermally stable and prominent in the dark-adapted OEC, while the S_4 state formed after the third flash immediately decays to the S_0 state in the dark, concurrent with release of an oxygen molecule (*1*, *2*). Inorganic cofactors, calcium and chloride ions, and Y_Z tyrosine have been suggested to play structural and/or functional roles in the OEC (*3*). A recent X-ray crystallographic model of the OEC at 3.5 Å resolution suggested that three Mn ions and one calcium ion are positioned in a cubane-like core connected to the fourth Mn ion (*4*). The metal ions were connected to each other by di-μ-oxo and mono-μ-oxo bridges, and carboxylates from Asp/Glu and imidazole from His were proposed as possible ligands.

Studies have thoroughly characterized the S-state-dependent changes in physical properties of the Mn cluster. Extended X-ray absorption fine structure (EXAFS) measurements showed no changes in the Mn−Mn distances of 2.7 Å for two di-μ-oxo bridges and 3.3 Å for one mono-μ-oxo bridge between the S_1 and S_2 states; however, the distances increased to 2.8−3.0 and 3.4 Å, respectively, in the S_3 state, indicating structural changes in the di-μ-oxo and mono-μ-oxo cores during the S_2-to-S_3 transition, but not during the S_1-to-S_2 transition (*5*). Results from X-ray absorption and emission spectroscopy indicate that the Mn cluster is oxidized in a stepwise manner during S_0-to-S_1 and S_1-to-S_2 transitions, and that accumulated oxidizing equivalents in the cluster are canceled by rereduction during the S_3-to-S_0 transition (*6*−*8*); however, direct oxidation of the Mn ion may not accompany the S_2-to-S_3 transition (*7*, *8*). Electron spin echo envelope modulation (ESEEM) and electron spin echo electron nuclear double resonance (ESE-ENDOR) studies on the S_2-state electron spin resonance (ESR) multiline signal suggested direct association of the substrate water with manganese ion (*9*−*11*). However, none of these can detect

† This research was supported by grants for the Frontier Research System and Special Postdoctoral Researchers Program at RIKEN.

* To whom correspondence should be addressed. Tel: +81 (22) 228 2047. Fax: +81 (22) 228 2045. E-mail: ykimura@postman.riken.go.jp, takaaki@postman.riken.go.jp.

‡ RIKEN.

§ Hiroshima University.

[1] Abbreviations: OEC, oxygen-evolving complex; PS, photosystem; Chl, chlorophyll; Mes, 2-(*N*-morpholino)ethanesulfonic acid; FTIR, Fourier transform infrared; NIR, near-infrared; EXAFS, extended X-ray absorption fine structure; XANES, X-ray absorption near edge structure; ESR, electron spin resonance; ESEEM, electron spin echo envelope modulation; ESE-ENDOR, electron spin echo electron nuclear double resonance.

10.1021/bi048203d CCC: $30.25
Published on Web 05/06/2005

directly the substrate water and/or its reaction intermediate bound to the Mn cluster, or the chemical nature of the interaction between them, and both are indispensable for understanding the chemistry involved in water oxidation.

Infrared spectroscopy is a powerful technique for detecting subtle changes in molecular structure and in chemical nature of bonds involved in chemical reactions, which can provide insights into the mechanism of biochemical processes (*12*). This method has been applied to the OEC for elaborating the mechanism of photosynthetic water oxidation by examining light-induced FTIR difference spectra during S-state cycling (*13*−*19*). Studies in the mid-frequency region (1800−800 cm^{-1}) demonstrated characteristic structural changes of protein matrices and amino acid side groups during S-state transitions (*13*−*15*, *17*−*19*); while high-frequency (3800−2150 cm^{-1}) spectra showed S-state-dependent changes in the OH vibrational mode of water molecules (*16*). These may include modes arising from amino acid ligands of the Mn cluster and from the substrate water molecules bound to the cluster. However, it is also feasible to consider that these are structurally coupled with the Mn cluster, but in an indirect manner. Metal−ligand vibrations appear at low frequencies, and therefore the direct detection of chemical bonding between the Mn cluster and its ligands, including substrate water molecules in the OEC, is possible using low-frequency vibrational spectroscopy. Low-frequency (650−350 cm^{-1}) FTIR (*20*−*22*) and near-infrared (NIR) excitation Raman (*23*) spectroscopy have been applied to the OEC for S_2/S_1 differences, and some bands were characterized on the basis of behavior upon labeling by stable isotopes. However, because of technical difficulties of detecting low-frequency vibrational modes, S-state cycling has not been evaluated using low-frequency spectroscopy.

Here, we report for the first time the complete set of low-frequency (670−350 cm^{-1}) and mid-frequency (1800−1100 cm^{-1}) FTIR difference spectra for S-state cycling in PS II core particles isolated from the thermophilic cyanobacterium *Thermosynechococcus elongatus*. Furthermore, we report low-frequency FTIR difference spectra during S-state cycling in the cores labeled with four water isotopes, $H_2{}^{16}O$, $H_2{}^{18}O$, $D_2{}^{16}O$, and $D_2{}^{18}O$, and characterize the effects of the respective water isotopes on FTIR spectra for each S-state transition. On the basis of the results, changes in the chemical nature of reaction intermediates derived from substrate water at each S-state transition during photosynthetic water oxidation are discussed.

MATERIALS AND METHODS

PS II Core Particles. The PS II core particles from *T. elongatus* were prepared as described previously (*24*), with modifications. Cells were photoautotrophically grown in DTN medium (*25*) at 52 °C. Harvested cells were stirred gently in medium (0.4 M mannitol, 50 mM K_2HPO_4/KH_2PO_4, pH 6.8) in the presence of 1.5 mg/mL lysozyme and 2 mM ethylenediaminetetraacetic acid at 40 °C for 2 h. The following procedures were conducted on ice unless noted. Lysozyme-treated cells were disrupted using Bead-Beater (Bio-Spec Products) in medium A (25% (v/v) glycerol, 10 mM $MgCl_2$, 10 mM $CaCl_2$, 40 mM Mes/NaOH, pH 6.5). The homogenate was centrifuged at 26300*g* for 30 min after dilution with medium A, and then the supernatant was centrifuged at 218000*g* for 1.5 h to precipitate the thylakoid membranes. The thylakoid membranes were solubilized in medium (20% (v/v) glycerol, 0.5 M mannitol, 10 mM $MgCl_2$, 10 mM $CaCl_2$, 20 mM Mes/NaOH, pH 6.5) with Zwittergent 3-12 at 1 mg of Chl/mL for 20 min at 20 °C as described previously (*24*). The amount of detergent was optimized for each batch of thylakoid membranes. After centrifugation at 257000*g* for 1.5 h, the PS II core particles in the supernatant were precipitated by centrifugation at 257000*g* for 1 h in the presence of 15% (w/v) poly(ethylene glycol) 6000. The core particles were solubilized in medium containing 10% (v/v) glycerol, 20 mM Mes/NaOH, 20 mM NaCl, and 1.2% (w/v) *n*-dodecyl β-D-maltoside (pH 6.5), applied to a Mono-Q HR10/10 column (Amersham Biosciences), and eluted with a linear NaCl gradient (100−400 mM) in 20 mM Mes/NaOH and 0.03% (w/v) *n*-dodecyl β-D-maltoside (pH 6.0). Medium of the core particle fraction was replaced with medium containing 5 mM NaCl, 5 mM $CaCl_2$, 0.03% (w/v) *n*-dodecyl β-D-maltoside, and 10 mM Mes/NaOH (pH 6.0) through repeated ultrafiltration, followed by storage in liquid N_2. The O_2 evolution activity of the PS II core particles obtained was ∼3500 μmol of O_2 (mg of Chl)$^{-1}$ h^{-1} at 25 °C using 3 mM potassium ferricyanide and 1 mM phenyl-*p*-benzoquinone as electron acceptors.

Samples for FTIR. For replacement of $H_2{}^{16}O$ with isotopic water ($H_2{}^{18}O$, $D_2{}^{16}O$, or $D_2{}^{18}O$), core particle suspensions (20 μL, 3.2−3.6 mg of Chl/mL) spread thin on a plastic plate were dried under a stream of N_2 gas at 4 °C for 6−9 min and resuspended in the same volume of $H_2{}^{18}O$ (95 atom % ^{18}O, Rotem Industries), $D_2{}^{16}O$ (99.9 atom % D, Aldrich), or $D_2{}^{18}O$ (95 atom % ^{18}O, 99 atom % D, ICON) followed by incubation at 6 °C in the dark over 20 h. Prolonged dark incubation with isotopic water did not affect the features of the light-induced FTIR spectra. *Thermosynechococcus* core particles were highly stable, and little activity loss was detected during these procedures.

Non-($H_2{}^{16}O$)-substituted, $H_2{}^{18}O$-, $D_2{}^{16}O$-, or $D_2{}^{18}O$-substituted core particle suspensions (7−9 μL, 3.2−3.6 mg of Chl/mL) were mixed with a $H_2{}^{16}O$, $H_2{}^{18}O$, $D_2{}^{16}O$, or $D_2{}^{18}O$ solution of sodium ferricyanide (1 μL, 100 mM stock) as an electron acceptor. The mixture was deposited on an AgCl or BaF_2 disk (20 mm diameter) for low- or mid-frequency measurement, and partially dried under a stream of N_2 gas (4 °C) for 7−10 min. After placing an aliquot (1 μL) of a $H_2{}^{16}O$, $H_2{}^{18}O$, $D_2{}^{16}O$, or $D_2{}^{18}O$ solution with glycerol (20% v/v) adjacent to each substituted core sample for controlling the $H_2{}^{16}O$, $H_2{}^{18}O$, $D_2{}^{16}O$, or $D_2{}^{18}O$ content (*16*, *18*), the sample on the disk was covered by another AgCl or BaF_2 disk using a greased Teflon spacer, and incubated at 0 °C in the dark for 1 h.

FTIR Measurements. Low-frequency (670−350 cm^{-1}) or mid-frequency (1800−1100 cm^{-1}) FTIR spectra were recorded at 4 cm^{-1} resolution using a Bomen MB102 spectrophotometer equipped with a Si bolometer (Infrared, HDL-5) or a Bruker IFS-66v/s spectrophotometer equipped with an MCT detector (EG&G Optoelectronics D316/6). Sample temperature was maintained at 0 °C (±0.03 °C) using a homemade cryostat and temperature controller (Chino, KP1000) (*18*). The same custom-made cryostat was used for measuring the low- and mid-frequency spectra, with the exception of the IR windows. Each dark-adapted sample was subjected to four or eight successive saturating flashes from

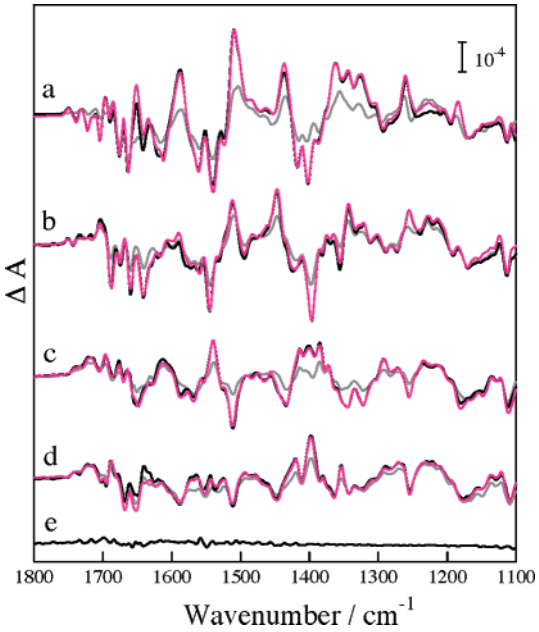

FIGURE 1: Effects of $H_2{}^{18}O$ substitution on mid-frequency (1800−1100 cm^{-1}) FTIR difference spectra during S-state cycling in PS II core particles from *T. elongatus*: (a) S_2/S_1, (b) S_3/S_2, (c) S_0/S_3, and (d) S_1/S_0 difference spectra of the nonsubstituted (black) and $H_2{}^{18}O$-substituted (magenta) core particles induced by the first-, second-, third-, and fourth-flash illumination, respectively. Gray lines show difference spectra induced by the (a) fifth-, (b) sixth-, (c) seventh-, and (d) eighth-flash illumination of the nonsubstituted core particles. Sample suspension included ferricyanide as an exogenous electron acceptor. The spectra were normalized with respect to the peak-to-peak intensity of the 2036(+) cm^{-1} band for ferrocyanide and the 2115(−) cm^{-1} band for ferricyanide (*22*). The $H_2{}^{18}O$-substituted spectra were scaled to minimize the difference from the nonsubstituted spectra. Spectrum e is presented to show the noise level.

a frequency-doubled Nd^{3+}:YAG laser (Spectra Physics INDI-50, 532 nm, pulse width 6−7 ns) at 10-s intervals. Single-beam spectra for the low-frequency region (7 scans) and mid-frequency region (20 scans) were measured before the first flash and after each successive flash, followed by dark adaptation for 30 min. This sequence was repeated 7−10 times before sample exchange. Flash-induced FTIR difference spectra for S-state transitions were obtained by subtracting the single-beam spectrum before each flash from that after the flash, and 275−290 or 26−34 difference spectra in the low- or mid-frequency region were averaged for each water isotope.

RESULTS

Mid-Frequency Spectra During S-State Cycling and Effects of $H_2{}^{18}O$ Substitution. Figure 1 shows flash-induced FTIR difference spectra in the mid-frequency region (1800−1100 cm^{-1}) of the nonsubstituted control PS II core particles upon the 1st−4th (black) and 5th−8th (gray) flashes, and of the $H_2{}^{18}O$-substituted core particles upon the 1st−4th (magenta) flashes. The difference spectra for the 1st-flash/dark, 2nd-flash/1st-flash, 3rd-flash/2nd-flash, and 4th-flash/3rd-flash correspond to those for S_2/S_1 (a), S_3/S_2 (b), S_0/S_3 (c), and S_1/S_0 (d) differences, respectively. The flash-number-dependent characteristic vibrational features were clearly evident over the first (1st−4th flashes) as well as second (5th−8th flashes) S-state cycling. Signal intensities for the second cycle were smaller and spectral features were vaguer

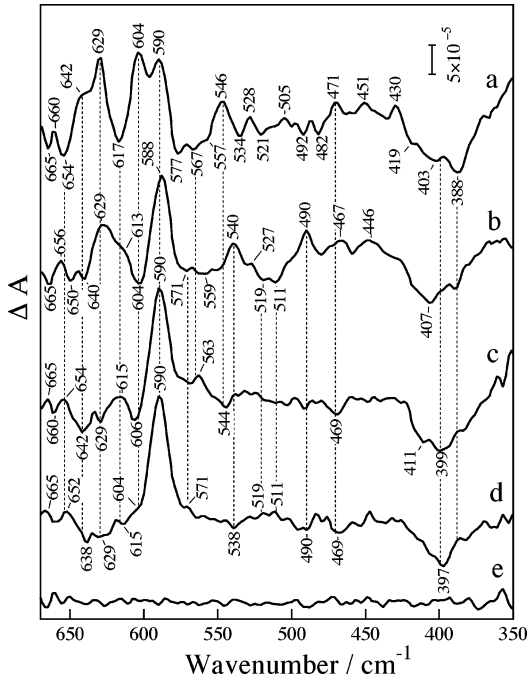

FIGURE 2: Low-frequency (670−350 cm^{-1}) FTIR difference spectra during S-state cycling in PS II core particles from *T. elongatus*: (a) S_2/S_1, (b) S_3/S_2, (c) S_0/S_3, and (d) S_1/S_0 difference spectra induced by the first-, second-, third-, and fourth-flash illumination, respectively. Sample suspensions included ferricyanide as an exogenous electron acceptor. The spectra were normalized with respect to the peak-to-peak intensity of the 590(+) cm^{-1} band for ferrocyanide and near 400(−) cm^{-1} for ferricyanide. Spectrum e is presented to show the noise level.

than those for the first cycle because of the scrambling of each S-state with approximately 15% of miss-hit. Bands at 1600−1500 cm^{-1} and 1450−1300 cm^{-1} correspond to the asymmetric and symmetric stretching modes, respectively, of the putative carboxylate ligands for the Mn cluster, while the amide I (1700−1600 cm^{-1}) and amide II (1600−1500 cm^{-1}) modes are attributed to polypeptide backbones. In general, these spectra are compatible with those previously reported for PS II preparations from spinach (*14*, *18*), and for core particles from histidine-tagged *Thermosynechococcus* (*13*, *15*−*17*, *19*) and *Synechocystis* (*18*) despite slight differences in peak positions and band intensities. Notably, the spectra induced upon the 1st- to the 4th-flash illumination in the $H_2{}^{18}O$-substituted OEC (magenta) overlapped with those in the nonsubstituted control OEC (black) almost completely, demonstrating that mid-frequency spectra for S-state cycling are largely insensitive to $H_2{}^{18}O$ substitution. These results indicate that the mid-frequency spectra include few vibrations related to the substrate water or from groups including oxygen atoms exchangeable with water oxygen.

Low-Frequency Spectra During S-State Cycling. Figure 2 shows flash-induced FTIR difference spectra in the low-frequency region (670−350 cm^{-1}) during S-state cycling. The PS II core particles from *Thermosynechococcus* were illuminated under conditions identical to those for the mid-frequency measurements. Therefore, spectra after the 1st-to-4th flash reflect S_2/S_1 (a), S_3/S_2 (b), S_0/S_3 (c), and S_1/S_0 (d) differences, respectively, corresponding to those in the mid-frequency range shown in Figure 1. Bands at ~400(−) cm^{-1} and 590(+) cm^{-1} in the difference spectra were ascribed to modes from the ferricyanide added as an electron

acceptor and ferrocyanide generated by the light-induced reduction of ferricyanide, respectively (*20*, *22*). These bands appeared with almost the same intensity after each flash, consistent with the equivalent appearance of the CN stretching bands of ferricyanide and ferrocyanide at 2115(−) and 2036(+) cm^{-1}, respectively, in the mid-frequency spectra (data not shown), supporting quantitative electron transfer from the Mn cluster to ferricyanide upon each flash illumination. Obviously, the spectral features changed markedly depending on flash number, with the exception of the ferrocyanide/ferricyanide bands, indicating that most of the bands directly reflect S-state dependent changes in the OEC. Spectra for the S_0/S_3 and S_1/S_0 differences appeared relatively featureless compared to those for S_2/S_1 and S_3/S_2, although some S-state-dependent bands were evident. However, this result is not ascribed to incomplete cycling of the S states because mid-frequency spectra obtained after the 3rd and 4th flashes under the same conditions clearly showed characteristic vibrational features for S_0/S_3 and S_1/S_0 differences, respectively (Figure 1). The low-frequency S_2/S_1 spectrum presented is comparable to those reported for another mesophilic cyanobacterium *Synechocystis* sp. PCC 6803 (*22*, *26*−*28*) or spinach (*20*, *21*), despite differences due to variations in sample preparation and/or experimental conditions. Notably, bands at 660(+), 654(−), 642(+), 629(+), 617(−), 604(+), 590(+), 577(−), 546(+), 534(−), 471(+), 430(+), 403(−), and 388(−) cm^{-1} appeared both in the S_2/S_1 spectrum reported here and in those reported previously. Most of these bands appeared to show considerable changes during S-state cycling. Notably, the main band features of the present S_3/S_2 spectrum are roughly compatible with those in the reported double difference spectrum for the S_3/S_2 difference, obtained by subtracting the 1st-flash/dark spectrum from the 2nd-flash/dark spectrum, in PS II core particles from spinach, although the S-state cycling was not examined (*29*).

Effects of $H_2{}^{18}O$ Substitution on Low-Frequency S-State Cycling Spectra. Figure 3 shows flash-induced low-frequency FTIR difference spectra for S_2/S_1 (a), S_3/S_2 (b), S_0/S_3 (c), and S_1/S_0 (d) differences of $H_2{}^{18}O$-substituted PS II core particles (magenta), together with those of the nonsubstituted core particles (black). Spectral features of the $H_2{}^{18}O$-substituted OEC were clearly different from those of the nonsubstituted control. In the spectra for S_2/S_1 (a), S_3/S_2 (b), S_0/S_3 (c), and S_1/S_0 (d) differences, the intensity and/or position of most bands in the 670−540 cm^{-1} range were substantially affected upon $H_2{}^{18}O$ substitution. In contrast, effects of substitution were less prominent in the 540−370 cm^{-1} bands although small but distinct differences were seen at 500−450 cm^{-1}. The significant effect of $H_2{}^{18}O$ substitution on the low-frequency spectra is in striking contrast to the mid-frequency spectra, which were minimally affected by substitution as shown in Figure 1. This implies that the low-frequency bands affected by the $H_2{}^{18}O$ substitution are not due to modes from amino acid side groups and protein backbones but to modes from the Mn cluster including the ligands. All the difference spectra included bands for ferrocyanide at 590(+) cm^{-1} and ferricyanide at ~400(−) cm^{-1}, which were insensitive to the water isotope although some S-state-dependent bands overlapped at these frequencies.

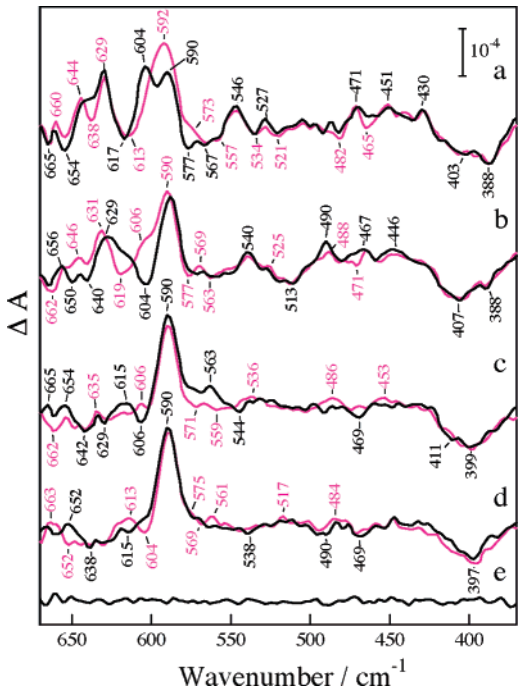

FIGURE 3: Effects of $H_2{}^{18}O$ substitution on low-frequency (670−370 cm^{-1}) FTIR difference spectra during S-state cycling in PS II core particles from *T. elongatus*: (a) S_2/S_1, (b) S_3/S_2, (c) S_0/S_3, and (d) S_1/S_0 difference spectra of the $H_2{}^{18}O$-substituted (magenta) and nonsubstituted (black) core particles induced by the first-, second-, third-, and fourth-flash illumination, respectively. Difference spectra of the nonsubstituted particles are reproduced from Figure 2. Spectrum e is presented to show the noise level.

Effects of $D_2{}^{16}O$ Substitution on Low-Frequency S-State Cycling Spectra. Figure 4 shows the flash-induced low-frequency FTIR difference spectra for S_2/S_1 (a), S_3/S_2 (b), S_0/S_3 (c), and S_1/S_0 (d) differences of $D_2{}^{16}O$-substituted PS II core particles (green), together with those of nonsubstituted core particles (black). S-state cycling spectra of $D_2{}^{16}O$-substituted particles were clearly different from those of nonsubstituted control spectra. The spectral features of S_2/S_1 (a) and S_0/S_3 (c) differences of the nonsubstituted OEC were substantially changed in intensity and/or position by $D_2{}^{16}O$ substitution. In particular, the $D_2{}^{16}O$-substituted S_0/S_3 difference spectrum showed a prominent negative band at 640 cm^{-1} where no intense band existed in the nonsubstituted spectra. In contrast, the S_3/S_2 (b) and S_1/S_0 (d) difference spectra in $D_2{}^{16}O$-substituted OEC largely overlapped with the nonsubstituted spectra except for minor differences. Effects of $D_2{}^{16}O$ substitution on S-state cycling spectra have been reported in the mid-frequency (1800−1200 cm^{-1}) and high-frequency (3800−2150 cm^{-1}) regions (*16*), in which characteristic isotopic effects were prominently observed in the spectrum for every transition. Therefore, the appearance of isotopic effects by $D_2{}^{16}O$ substitution at the specific S-state transitions (S_1-to-S_2 and S_3-to-S_0) in the present low-frequency spectra suggests that the low-frequency modes affected by deuteration are ascribed to species that appeared and/or disappeared during these two transition processes. Furthermore, the manifestation of S-state-dependent isotopic effects during the S-state cycling was markedly different in $H_2{}^{18}O$ and $D_2{}^{16}O$ substitutions; marked isotopic effects were observed for oxygen but not for hydrogen for the S_3/S_2 difference. Under the present experimental conditions, it may be possible that the D_2O-

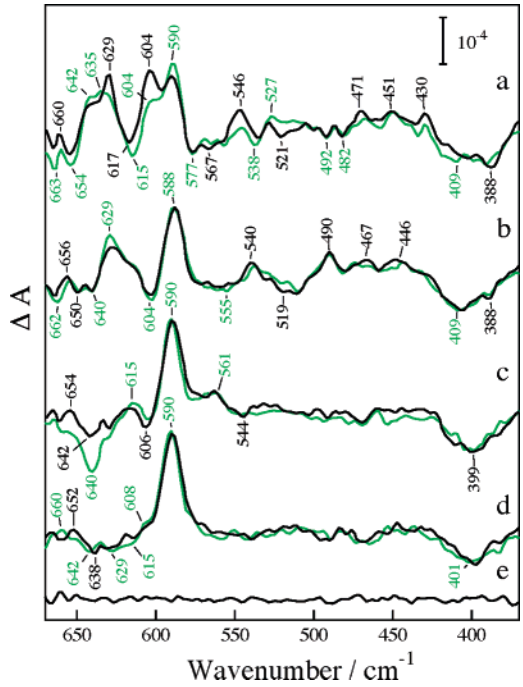

FIGURE 4: Effects of $D_2{}^{16}O$ substitution on low-frequency (670−370 cm^{-1}) FTIR difference spectra during S-state cycling in PS II core particles from *T. elongatus*: (a) S_2/S_1, (b) S_3/S_2, (c) S_0/S_3, and (d) S_1/S_0 difference spectra of the $D_2{}^{16}O$-substituted (green) and nonsubstituted (black) core particles induced by the first-, second-, third-, and fourth-flash illumination, respectively. Difference spectra of the nonsubstituted particles are reproduced from Figure 2. Spectrum e is presented to show the noise level.

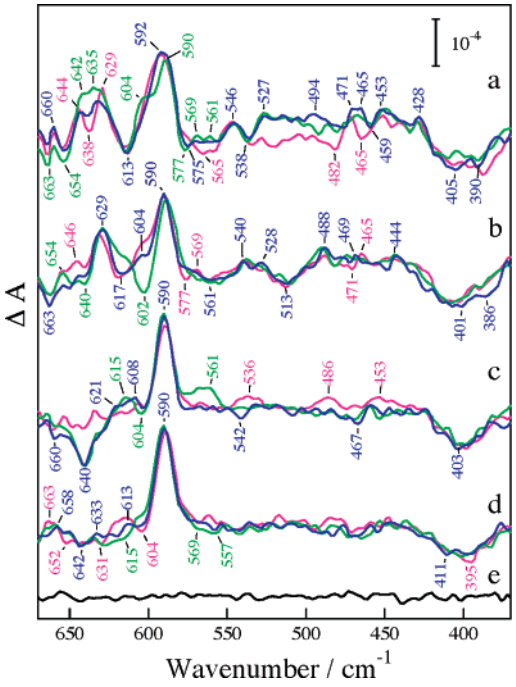

FIGURE 5: Effects of $D_2{}^{18}O$ substitution on low-frequency (670−370 cm^{-1}) FTIR difference spectra during S-state cycling in PS II core particles from *T. elongatus*: (a) S_2/S_1, (b) S_3/S_2, (c) S_0/S_3, and (d) S_1/S_0 difference spectra of the $D_2{}^{18}O$-substituted (blue), $H_2{}^{18}O$-substituted (magenta), and $D_2{}^{16}O$-substituted (green) core particles induced by the first-, second-, third-, and fourth-flash illumination, respectively. Difference spectra of the $H_2{}^{18}O$-substituted and $D_2{}^{16}O$-substituted particles are reproduced from Figures 3 and 4, respectively. Spectrum e is presented to show the noise level.

induced change in the medium pH (∼0.5) influences IR bands for the amino acid side chains and/or polypeptide backbones. However, no obvious pH dependence was reported in the mid-frequency spectra for the S-state cycling at pH 6−8 (*19*), indicating that possible pH-shift by the $D_2{}^{16}O$ substitution little affects low-frequency vibrational modes for these species.

Effects of $D_2{}^{18}O$ Substitution on Low-Frequency S-State Cycling Spectra. Figure 5 shows the flash-induced low-frequency FTIR difference spectra for S_2/S_1 (a), S_3/S_2 (b), S_0/S_3 (c), and S_1/S_0 (d) differences of $D_2{}^{18}O$-substituted PS II core particles (blue), together with those of $H_2{}^{18}O$-(magenta) and $D_2{}^{16}O$-substituted (green) core particles. In general, characteristic isotopic changes for both ^{18}O in the $H_2{}^{18}O$-substituted spectra and D in the $D_2{}^{16}O$-substituted spectra were cumulatively induced in the $D_2{}^{18}O$-substituted spectra. Spectral features for the S_2/S_1 and S_3/S_2 differences in the $D_2{}^{18}O$-substituted spectra were considerably different from those in the $D_2{}^{16}O$-substituted spectra at 670−550 cm^{-1}, but were not much different below 550 cm^{-1}. Some characteristic variations were also apparent between $D_2{}^{18}O$- and $H_2{}^{18}O$-substituted spectra for the S_2/S_1 and S_0/S_3 differences. A prominent negative band at 640 cm^{-1} was evident for the S_0/S_3 difference similar to the $D_2{}^{16}O$-substituted spectrum. Furthermore, a positive band at 561 cm^{-1} in the S_0/S_3 difference spectra of $D_2{}^{16}O$-substituted as well as non-($H_2{}^{16}O$)-substituted (Figures 3 and 4, black) particles was not induced in both $D_2{}^{18}O$- and $H_2{}^{18}O$-substituted spectra.

Low-Frequency Vibrations Related to Oxygen and/or Hydrogen from Water. To inspect and evaluate the effects of isotopic exchange by water oxygen, the $H_2{}^{16}O/H_2{}^{18}O$ or $D_2{}^{16}O/D_2{}^{18}O$ double difference spectrum was obtained by subtracting the $H_2{}^{18}O$- or $D_2{}^{18}O$-substituted spectrum from the non-($H_2{}^{16}O$)- or the $D_2{}^{16}O$-substituted spectrum, respectively, for each S-state transition. Figure 6 shows the $H_2{}^{16}O/H_2{}^{18}O$ (magenta) and $D_2{}^{16}O/D_2{}^{18}O$ (blue) double difference spectra for S-state cycling. Basically, overall spectral features of both double difference spectra were very similar for each S-state difference. Prominent isotopic bands were observed in the double difference spectra for S_2/S_1 (a) and S_3/S_2 (b) differences, and medium-intensity bands were seen for the S_1/S_0 (d) difference, while relatively small bands appeared for the S_0/S_3 (c) difference. Bands at 638(+)/617(−)/606(+)/594(−), 635(−)/621(+)/602(−)/582(+), 636(−)/615(+)/606(−)/563(+), and 615(−)/606(+)/596(+) cm^{-1} were induced consistently in both the $H_2{}^{16}O/H_2{}^{18}O$ and $D_2{}^{16}O/D_2{}^{18}O$ double difference spectra for the S_2/S_1, S_3/S_2, S_0/S_3, and S_1/S_0 differences, respectively. These results show that modes including the interactions between oxygen and hydrogen do not much contribute to the low-frequency spectra. Therefore, it is indicated that large portions of the structural constituents and/or chemical species responsible for the ^{18}O-water sensitive bands do not include structurally coupled hydrogen that can exchange with water hydrogen. In addition, bands at 617(−), 606(+), and 594(−) cm^{-1} in the S_2/S_1 double difference spectra appeared to show S-state-dependent changes in sign and intensity, suggesting that periodic structural changes of the groups including exchangeable oxygen are partly responsible for the S-state-dependent bands. In contrast, distinctive differences were evident at 670−640 cm^{-1} in the $H_2{}^{16}O/H_2{}^{18}O$ and $D_2{}^{16}O/D_2{}^{18}O$ double difference spectra for the S_2/S_1, S_3/S_2, or S_1/S_0 difference.

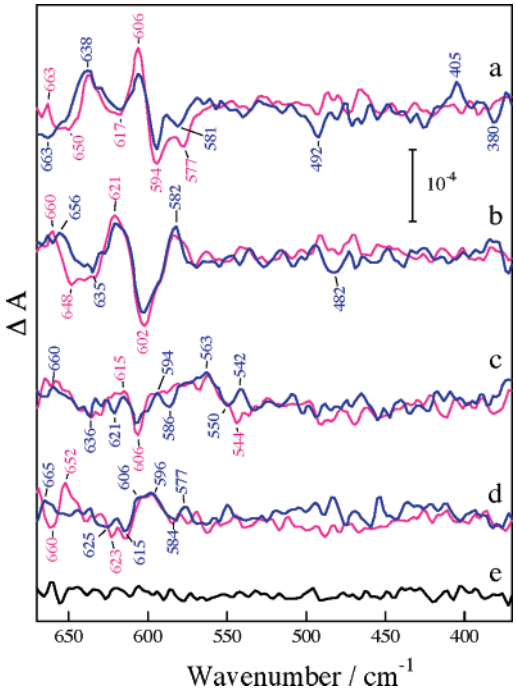

FIGURE 6: Effects of ^{16}O-water/^{18}O-water exchange on low-frequency (670−370 cm^{-1}) FTIR difference spectra for the (a) S_2/S_1, (b) S_3/S_2, (c) S_0/S_3, and (d) S_1/S_0 differences in PS II core particles from *T. elongatus*. $H_2{}^{16}O/H_2{}^{18}O$ (magenta) double difference spectra were obtained by subtracting the $H_2{}^{18}O$-substituted S-state difference spectra (Figure 3, magenta) from the non-($H_2{}^{16}O$)-substituted S-state difference spectra (Figure 3, black). $D_2{}^{16}O/D_2{}^{18}O$ (blue) double difference spectra were obtained by subtracting the $D_2{}^{18}O$-substituted S-state difference spectra (Figure 5, blue) from the $D_2{}^{16}O$-substituted S-state difference spectra (Figure 5, green). Difference spectra were scaled to minimize respective double differences. Spectrum e is presented to show the noise level for the double subtraction.

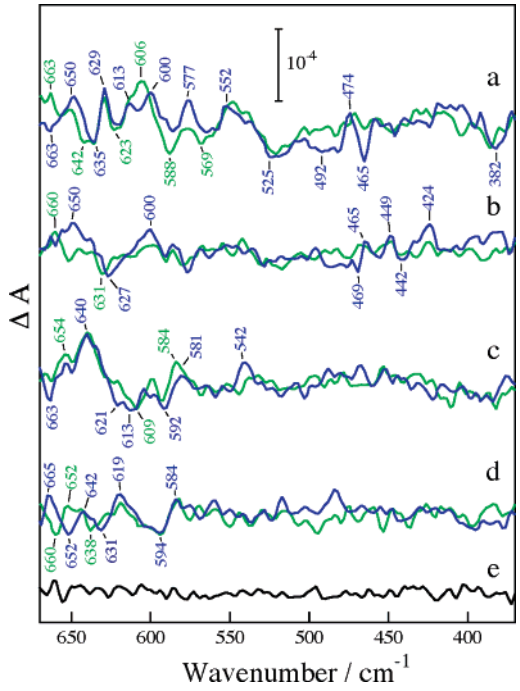

FIGURE 7: Effects of H-water/D-water exchange on low-frequency (670−370 cm^{-1}) FTIR difference spectra for the (a) S_2/S_1, (b) S_3/S_2, (c) S_0/S_3, and (d) S_1/S_0 differences in PS II core particles from *T. elongatus*. $H_2{}^{16}O/D_2{}^{16}O$ (green) double difference spectra were obtained by subtracting the $D_2{}^{16}O$-substituted S-state difference spectra (Figure 4, green) from the non-($H_2{}^{16}O$)-substituted S-state difference spectra (Figure 4, black). $H_2{}^{18}O/D_2{}^{18}O$ (blue) double difference spectra were obtained by subtracting the $D_2{}^{18}O$-substituted S-state difference spectra (Figure 5, blue) from the $H_2{}^{18}O$-substituted S-state difference spectra (Figure 5, magenta). Difference spectra were scaled to minimize respective double differences. Spectrum e is presented to show the noise level for the double subtraction.

In addition, minor bands at 500−370 cm^{-1} appeared different in the two double difference spectra. Note that the reported ^{16}O/^{18}O double difference spectrum for the S_2/S_1 difference (*20*) exhibited relatively simple features comprising a 609(+)/596(−) cm^{-1} band pair and a smaller negative band at 625 cm^{-1}. These changes were proposed to be ascribed to isotope shifts of a single Mn−O−Mn mode, with a frequency that decreased upon oxidation of the Mn cluster during the S_1-to-S_2 transition. The present double difference spectrum revealed more bands, indicating that several bands affected by the ^{18}O-water exist in this region.

Bands affected by H/D exchange are seen clearly in the $H_2{}^{16}O/D_2{}^{16}O$ (green) and $H_2{}^{18}O/D_2{}^{18}O$ (blue) double difference spectra for the S_2/S_1 (a), S_3/S_2 (b), S_0/S_3 (c), and S_1/S_0 (d) differences as shown in Figure 7. The S_2/S_1 double difference spectra showed many isotopic bands that contained significant differences between the $H_2{}^{16}O/D_2{}^{16}O$ and $H_2{}^{18}O/D_2{}^{18}O$ double difference spectra. However, bands at 635(−)/629(+)/552(+)/525(−) cm^{-1} appeared consistently in both of the double difference spectra. For the S_3/S_2 difference, only a few, small $H_2{}^{16}O/D_2{}^{16}O$ isotopic bands were induced, whereas the $H_2{}^{18}O/D_2{}^{18}O$ double difference spectrum showed several isotopic bands at 670−550 cm^{-1} and 500−400 cm^{-1}. Notably, the $H_2{}^{16}O/D_2{}^{16}O$ and $H_2{}^{18}O/D_2{}^{18}O$ double difference spectra showed prominent isotopic bands at 654(+), 640(+), 609(−), and 592(−) cm^{-1} for the S_0/S_3 difference, although minor differences were observed between both double difference spectra at approximately 663(−), 621(−), 584(+), and 542(+) cm^{-1}. The marked H/D isotopic bands for the S_0/S_3 difference contrasted with minimal ^{16}O/^{18}O isotopic bands in the $H_2{}^{16}O/H_2{}^{18}O$ and $D_2{}^{16}O/D_2{}^{18}O$ double difference spectra (Figure 6). The S_1/S_0 double difference spectra showed many $H_2{}^{16}O/D_2{}^{16}O$ and $H_2{}^{18}O/D_2{}^{18}O$ isotopic bands in which only 619(+), 594(−), and 584 (+) cm^{-1} bands appeared consistently in both double difference spectra, indicating that most of the chemical species/structures responsible for H/D-sensitivity retain structurally coupled oxygen that is exchangeable with water oxygen. It is of note that the S-state-dependent appearance of the isotopic bands for water hydrogen ($H_2{}^{16}O/D_2{}^{16}O$ difference) was considerably different from that for water oxygen ($H_2{}^{16}O/H_2{}^{18}O$ difference). These differences probably reflect different isotopic effects on the chemical species involved in the reaction process for each transition step of water oxidation.

DISCUSSION

S-State-Dependent Low-Frequency Modes. Low-frequency (670−370 cm^{-1}) FTIR measurements for S-state cycling of the OEC demonstrate that the advancement of each reaction step of the intermediate S states results in markedly different spectra containing characteristic low-frequency bands that change their sign and intensity depending on each S-state transition as shown in Figure 2. IR bands in this frequency

Table 1: FTIR Bands Affected by Water Isotopes and Predominant Assignments

category	band positions/cm^{-1} S_2/S_1	S_3/S_2	S_0/S_3	S_1/S_0	predominant assignments
I(^{16}O/^{18}O)	638(+)	635(−)	636(−)	615(−)	MnO_2Mn, MnOMn, Mn_3O, Mn═O
	617(−)	621(+)	615(+)	606(+)	
	606(+)	602(−)	606(−)	596(+)	
	594(−)	582(+)	563(+)		
II (H/D)	635(−)	nd[a]	654(+)	619(+)	amino acid side chain, polypeptide backbone
	629(+)		640(+)	594(−)	
	552(+)		609(−)	584(+)	
	525(−)		592(−)		
III[b] (^{16}O/^{18}O, H/D)	~663	~650	~621	~662	$MnOH_2$, MnOH, MnO···H
	~644	~625	~606	~652	
	~608		~586		
	~590		~542		

[a] Not detected. [b] Bands were evaluated from the difference between $H_2{}^{16}O/H_2{}^{18}O$ (magenta) and $D_2{}^{16}O/D_2{}^{18}O$ (blue) double difference spectra in Figure 6, and therefore presented with no sign.

region arise from vibrational modes of Mn cluster cores and bonds between Mn ion and its ligands, including substrate water molecules and reaction derivatives as well as from vibrational modes of amino acids and polypeptide backbones associated with the Mn cluster. The 606 cm^{-1} band (604 cm^{-1} band in the present study), assigned to the Mn−O−Mn core mode in the S_2 state (*20*), changed sign and intensity during S-state cycling, indicating S-state-dependent changes in the core structure of the Mn cluster. In addition, the 642 cm^{-1} band, affected by L-[1-^{13}C]alanine (*28*) as well as universal ^{13}C-labeling (*22*) in the S_2/S_1 spectrum, appeared positively in the S_2/S_1 spectrum and negatively in the S_0/S_3 spectrum, while few bands were observed in S_3/S_2 and S_1/S_0 spectra (Figure 2). Interestingly, this S-state dependency is compatible with that of mid-frequency stretching modes of α-carboxylates of D1 C-terminal Ala334, which ligate Mn ion oxidized during S_1-to-S_2 transition and reduced during S_3-to-S_0 transition (*28*). Therefore, structural changes of the D1 C-terminal Ala344 α-carboxylate are likely attributable to the 642 cm^{-1} band, of which possible vibrational assignment is out-of-plane [π(COO)] or in-plane [δ(OCO)] bending modes (*30*, *31*).

Another remarkable result of the present study was that the low-frequency S-state spectra observed were significantly and differently affected by water isotopes, including ^{18}O and/or deuterium. The ^{16}O/^{18}O- and/or H/D-sensitive vibrational modes detected in low-frequency spectra during S-state cycling can be ascribed to structures that retain and/or associate with oxygen and/or hydrogen exchangeable with those of water molecules in the reaction process of the photosynthetic water oxidation. Although detailed one-to-one assignment of the ^{16}O/^{18}O- and/or H/D-sensitive bands for the respective S states is not feasible at present, S-state dependencies provide useful information on the types of structural and/or chemical changes that accompany each S-state transition. The major bands affected by water isotopes in each S-state transition are classified into three categories as summarized in Table 1.

^{16}O/^{18}O-Water-Sensitive but H/D-Water-Insensitive Bands. The first category (category I) includes bands that commonly appeared at the same position in both $H_2{}^{16}O/H_2{}^{18}O$ (magenta) and $D_2{}^{16}O/D_2{}^{18}O$ (blue) double difference spectra, as shown in Figure 6. These bands were affected by ^{16}O/^{18}O exchange but not by H/D exchange, and were ascribed to chemical structures/species that retain oxygen exchangeable with water oxygen, but do not involve structurally coupled hydrogen exchangeable with water hydrogen. Apparently, low-frequency modes reflecting interactions between water vibrations and amino acid side chains/polypeptide backbones usually do not contribute to these bands. This view is consistent with observations that none of the bands in the mid-frequency spectra for S-state cycling were sensitive to $H_2{}^{18}O$ substitution, as shown in Figure 1. In addition, interactions between Mn and substrate water including its reaction derivatives retaining hydrogen also were excluded from contributing to these bands because these modes are affected by H/D exchange (*32*). Therefore, direct interactions between water-derived oxygen and Mn ions in the cluster are responsible for this category of bands. Notably, most of the prominent ^{16}O/^{18}O-sensitive bands observed during the S-state cycling belonged to this category. Such bands were detected at 638(+)/617(−)/606(+)/594(−), 635(−)/621(+)/602(−)/582(+), 636(−)/615(+)/606(−)/563(+), and 615(−)/606(+)/596(+) cm^{-1} for the S_2/S_1, S_3/S_2, S_0/S_3, and S_1/S_0 differences, respectively. The low-frequency S_2/S_1 and S_3/S_2 spectra and the effects of $H_2{}^{18}O$ substitution on the spectra were reported in core preparations of spinach (*20*, *29*), in which the 606 cm^{-1} and ~621 cm^{-1} bands affected by $H_2{}^{18}O$ substitution were tentatively assigned to Mn cluster core modes in the S_2 and S_3 states, respectively. Apparently, category I bands contribute mainly to these two bands. Possible candidates for species responsible for these ^{16}O/^{18}O isotopic bands are Mn cluster cores involving bridging oxygen: $Mn_2(\mu\text{-O})_2$ (*33*−*38*), $Mn_2(\mu\text{-O})$ (*37*, *39*), and Mn_3O (*30*, *40*, *41*). These oxygen species may be purely structural constituents of the Mn cluster, although the ability of structural oxygen in the Mn cluster to exchange with water oxygen is unknown. These oxygen species not only may be structural constituents but also may participate in the chemistry of water oxidation directly, and thus are exchangeable with water oxygen. It was hypothesized that these types of oxygen species are responsible for the water intermediates slowly exchangeable with ^{18}O-water (*42*), based on kinetic mass spectrometric detection of O_2 including ^{18}O derived from ^{18}O-water which was introduced to the sample in a particular S state (*43*). Alternatively, the chemical bond between high-valence Mn and oxygen from substrate (i.e. Mn(IV)═O) may be involved in water oxidation before O−O bond formation (*44*). Therefore, terminal Mn═O species (*45*−*48*) derived from substrate water also are possible candidates for bands sensitive only to ^{16}O/^{18}O exchange, although recent XANES studies report the absence of Mn═O species in the S_3 state (*49*).

H/D-Water-Sensitive but ^{16}O/^{18}O-Water-Insensitive Bands. The second category (category II) includes bands affected only by H/D exchange, which commonly appeared at the same position in both the $H_2{}^{16}O/D_2{}^{16}O$ (green) and $H_2{}^{18}O/D_2{}^{18}O$ (blue) double difference spectra, shown in Figure 7. These bands can be ascribed to modes from amino acid side chains and polypeptide backbones associated with exchangeable hydrogen but not with exchangeable oxygen in hydrophilic environments. Possible candidates for these bands include imidazole groups of histidine (*50*) and carboxylate groups of acidic amino acids as well as O═C−N

bending (amide IV), N−H out-of-plane bending (amide V), and C═O out-of-plane bending modes (amide VI) of polypeptides (*51*). The effects of universal ^{13}C- and ^{15}N-labeling on low-frequency S_2/S_1 spectra (*22*) indicate the likelihood that carbon-containing but not nitrogen-containing groups associated with the Mn cluster are mainly responsible for bands in the 640−600 cm^{-1} region. Modes in this region may also be caused by Mn cluster cores in which bridged oxygen is not exchangeable with water oxygen but interacts with hydrogen exchangeable with water hydrogen. EXAFS studies proposed the presence of a hydroxo bridge in the Mn cluster core (*52*), which may be responsible for category II bands when the oxygen is not exchangeable with water oxygen. The category II bands appeared at 635(−)/629(+)/552(+)/525(−), 654(+)/640(+)/609(−)/592(−), and 619(+)/594(−)/584(+) cm^{-1} for the S_2/S_1, S_0/S_3, and S_1/S_0 differences, respectively, but were not evident for the S_3/S_2 difference. Changes in sign and/or intensity of the category II bands were difficult to follow during the S-state cycling, in contrast to the $^{16}O/^{18}O$-sensitive category I bands. In particular, a significant category II band was induced at 640(+) cm^{-1} for the S_0/S_3 difference, as shown in Figure 7. Since the S_3-to-S_0 transition is accompanied by the release of two protons as well as an oxygen molecule (*53*), these changes may be responsible for the prominent appearance of category II bands for the S_0/S_3 difference. It is of note that changes in protonation state other than PS II components, such as buffer molecules (*18*), do not contribute to the low-frequency spectra presented here.

$^{16}O/^{18}O$-Water- and H/D-Water-Sensitive Bands. The third category (category III) includes bands affected by both $^{16}O/^{18}O$ and H/D exchanges; bands appeared differently between the $H_2{}^{16}O/H_2{}^{18}O$ (magenta) and $D_2{}^{16}O/D_2{}^{18}O$ (blue) double difference spectra shown in Figure 6. These bands are due to chemical species/structures that retain both oxygen and hydrogen structurally coupled to each other as well as exchangeable with oxygen and hydrogen in water molecules, since $^{16}O/^{18}O$ exchange leads the different spectral changes in light and heavy water, when structural coupling existed between hydrogen and oxygen. The category III bands also can be equivalently evaluated by comparing the $H_2{}^{16}O/D_2{}^{16}O$ (green) with $H_2{}^{18}O/D_2{}^{18}O$ (blue) double difference spectra, as shown in Figure 7. Such bands were seen around 663/644/608/590, 650/625, 621/606/586/542, and 662/652 cm^{-1} for S_2/S_1, S_3/S_2, S_0/S_3, and S_1/S_0 differences, respectively. The category III bands appeared at variously different frequencies depending on the S-state differences. This may reflect different chemical intermediates and/or interactions of them with the Mn cluster during S-state cycling. The possible origin of these bands lies with water-derived reaction intermediates associated with the Mn cluster. Candidates for these bands include Mn−O stretching modes of $Mn-OH_2$ and/or Mn−OH species with Mn(III) and/or Mn(IV), and a wagging mode of Mn-bound water (*32*). Hydrogen bonding between Ca^{2+}-bound water and a $Mn_2(\mu\text{-}O)_2$ unit (*54*) or protonation of a $Mn_2(\mu\text{-}O)_2$ unit (*52*) was assumed on the basis of EXAFS studies. If the bridging oxygen was exchangeable with water oxygen and interacted with hydrogen derived from water molecules, the bands for these structures were affected by both $^{16}O/^{18}O$ and H/D exchanges and contribute to the category III bands. It is of note in this context that category III bands may include the modes of $Ca-OH_2$ and/or Ca−OH species, although no relevant data have been available for these low-frequency modes. ESEEM and ESE-ENDOR studies suggested the association of water (*9*−*11*) and/or hydroxyl ligands (*11*) with paramagnetic Mn within the cluster in the S_0 and/or S_2 states. Time-resolved mass spectrometry indicated that the S_2 state OEC already binds two substrate water molecules (*55*). In addition, high-frequency (3800−2150 cm^{-1}) FTIR studies revealed that the S-state-dependent as well as $^{16}O/^{18}O$- and H/D-sensitive bands from water appear in the weakly H-bonded OH region (*16*). The water-derived modes proposed in these studies may contribute to the category III bands observed in the respective S states.

NIR excitation Raman spectroscopy (*23*) detected H/D-sensitive low-frequency S_1 modes at 476 and 438 cm^{-1}, which were tentatively assigned to the Mn−OH and/or $Mn-OH_2$ modes. In the present study, several minor but distinctive differences were found between double difference spectra in the region below 500 cm^{-1} as shown in Figures 6 and 7, suggesting that these bands may be due to interactions between Mn and OH/OH_2. Although the primary candidates for the origins of category III bands are substrate water associated with the Mn cluster and/or the intermediate species derived from the substrate, we cannot completely exclude the possibility that some $^{16}O/^{18}O$- and H/D-sensitive bands may be due to vibrations of water molecules associated with amino acid residues and/or polypeptides through hydrogen bond networks in some special manner, or that a slight pH change induced by the $D_2{}^{16}O$ substitution may affect the modes of $MnOH_2$ and/or MnOH species.

S-State Dependence of Bands from Water Isotopes. The low-frequency bands associated with water exhibited characteristic changes during S-state cycling, and this S-state dependency varied markedly among the categories of the bands. Category I bands, which commonly appeared both in the $H_2{}^{16}O/H_2{}^{18}O$ (magenta) and $D_2{}^{16}O/D_2{}^{18}O$ (blue) double difference spectra (Figure 6), were prominent in the double difference spectra for the S_2/S_1 (spectra a) and S_3/S_2 differences (spectra b), and were present in the S_1/S_0 difference (spectra d) but at lower intensity, probably due to the miss-hits during S-state cycling; the S_0-to-S_1 transition upon the fourth flash occurred in approximately 50% center considering the 15% miss-hits. In contrast, the S_3-to-S_0 transition was accompanied by the appearance of a few category I bands with reduced intensity (spectra c). On the basis of X-ray absorption spectroscopic studies, the S_1-to-S_2 transition involves oxidation of manganese ion from Mn(III) to Mn(IV), but little change in the Mn−Mn distances within the cluster (*5*−*8*). However, the S_2-to-S_3 transition involves significant changes in Mn−Mn distances (*5*) with no change in manganese valence (*7*, *8*, but see ref *6*). In model Mn complexes (*30*, *33*−*41*, *56*), modes from Mn−O interactions are significantly affected by the oxidation state of the manganese ion(s), although the direction and amplitude of the shifts observed in the corresponding IR bands varied among the complexes due to accompanying changes in symmetry of the complexes and differences in the nature of ligands. Therefore, changes in the oxidation state of the manganese ion and in the core structure of the Mn cluster may be responsible for the category I bands in the S_2/S_1 and S_3/S_2 difference spectra, respectively. Presumably, these two types of bands overlap and cannot be detected as individual

bands in the double difference spectra for the S_3-to-S_0 transition, in which changes in the structure and oxidation state of the Mn cluster occurring during the S_1-to-S_2 and S_2-to-S_3 transitions are reversed. Notably, category I bands dominated the bands in the 620−580 cm^{-1} region and appeared opposite each other in the S_3/S_2 and S_1/S_0 difference (Figure 6). Previous EXAFS studies reported that Mn−Mn distances in the cluster increase upon the S_2-to-S_3 transition (*5*), and one of the di-μ-oxo-bridged Mn−Mn moieties decreased from 2.85 to 2.7 Å upon the S_0-to-S_1 transition (*57*). Therefore, the expansion and shrinking of Mn cluster cores may be responsible for the portion of the category I bands from the S_2-to-S_3 and S_0-to-S_1 transitions, respectively.

Substrate water oxygen has been shown to be incorporated into the active site within the Mn cluster core structure in the S_0 state (*42*). Therefore, interactions between Mn and water-derived species are included in the present low-frequency FTIR spectra as category I and/or category III bands. These bands may be expected to show no obvious periodic changes depending on the S state in contrast to bands reflecting S-state-dependent change in the structure and/or oxidation states of the Mn cluster, because respective chemical intermediates show specific bands independently in each S-state spectrum. Notably, most of the category III bands were specific for each S-state transition, making it difficult to evaluate transition-dependent changes in their sign and intensity. The behavior of category III bands is compatible with a contribution of water and/or water-derived intermediates associated with the Mn cluster to the category III bands.

ACKNOWLEDGMENT

We thank Dr. Masahiko Ikeuchi and Dr. Tsunenori Nozawa for the gift of *T. elongatus* cells.

REFERENCES

1. Joliot, P., Barbieri, G., and Chabaud, R. (1969) Un nouveau modele des centres photochimiques du systeme II, *Photochem. Photobiol. 10*, 309−329.
2. Kok, B., Forbush, B., and McGloin, M. P. (1970) Cooperation of charges in photosynthetic O_2 evolution: 1. A linear four-step mechanism, *Photochem. Photobiol. 11*, 457−475.
3. Debus, R. J. (1992) The manganese and calcium ions of photosynthetic oxygen evolution, *Biochim. Biophys. Acta 1102*, 269−352.
4. Ferreira, K. N., Iverson, T. M., Maghlaoui, K., Barber, J., and Iwata, S. (2004) Architecture of the photosynthetic oxygen-evolving center, *Science 303*, 1831−1837.
5. Liang, W., Roelofs, T. A., Cinco, R. M., Rompel, A., Latimer, M. J., Yu, Wa O., Sauer, K., Klein, M. P., and Yachandra, V. K. (2000) Structural change of the Mn cluster during the $S_2 \rightarrow S_3$ state transition of the oxygen-evolving complex of photosystem II. Does it reflect the onset of water/substrate oxidation? Determination by Mn x-ray absorption spectroscopy, *J. Am. Chem. Soc. 122*, 3399−3412.
6. Ono, T.-A., Noguchi, T., Inoue, Y., Kusunoki, M., Matsushita, T., and Oyanagi, H. (1992) X-ray-detection of the period-4 cycling of the manganese cluster in photosynthetic water oxidizing enzyme, *Science 258*, 1335−1337.
7. Roelofs, T. A., Liang, W., Latimer, M. J., Cinco, R. M., Rompel, A., Andrews, J. C., Sauer, K., Yachandra, V. K., and Klein, M. P. (1996) Oxidation states of the manganese cluster during the flash-induced S-state cycle of the photosynthetic oxygen-evolving complex, *Proc. Natl. Acad. Sci. U.S.A. 93*, 3335−3340.
8. Messinger, J., Robblee, J. H., Bergmann, U., Fernandez, C., Glatzel, P., Visser, H., Cinco, R. M., McFarlane, K. L., Bellacchio, E., Pizarro, S. A., Cramer, S. P., Sauer, K., Klein, M. P., and Yachandra, V. K. (2001) Absence of Mn-centered oxidation in the $S_2 \rightarrow S_3$ transition: implications for the mechanism of photosynthetic water oxidation, *J. Am. Chem. Soc. 123*, 7804−7820.
9. Turconi, S., MacLachlan, D. J., Bratt, P. J., Nugent, J. H. A., and Evans, M. C. W. (1997) Analysis of the interaction of water with the manganese cluster of photosystem II using isotopically labeled water, *Biochemistry 36*, 879−885.
10. Evans, M. C. W., Nugent, J. H. A., Ball, R. J., Muhiuddin, I., and Pace, R. J. (2004) Evidence for a direct manganese−oxygen ligand in water binding to the S_2 state of the photosynthetic water oxidation complex, *Biochemistry 43*, 989−994.
11. Britt, R. D., Campbell, K. A., Peloquin, J. M., Gilchrist, M. L., Aznar, C. P., Dicus, M. M., Robblee, J., and Messinger, J. (2004) Recent pulsed EPR studies of the photosystem II oxygen-evolving complex: implications as to water oxidation mechanisms, *Biochim. Biophys. Acta 1655*, 158−171.
12. Bath, A., and Zscherp, C. (2002) What vibrations tell about proteins, *Q. Rev. Biophys. 35*, 369−430.
13. Noguchi, T., and Sugiura, M. (2001) Flash-induced Fourier transform infrared detection of the structural changes during the S-state cycle of the oxygen-evolving complex in photosystem II, *Biochemistry 40*, 1497−1502.
14. Hillier, W., and Babcock, G. T. (2001) S-state dependent Fourier transform infrared difference spectra for the photosystem II oxygen evolving complex, *Biochemistry 40*, 1503−1509.
15. Noguchi, T., and Sugiura, M. (2002) Flash-induced FTIR difference spectra of the water oxidizing complex in moderately hydrated photosystem II core films: effect of hydration extent on S-state transitions, *Biochemistry 41*, 2322−2330.
16. Noguchi, T., and Sugiura, M. (2002) FTIR detection of water reactions during the flash-induced S-state cycle of the photosynthetic water-oxidizing complex, *Biochemistry 41*, 15706−15712.
17. Noguchi, T., and Sugiura, M. (2003) Analysis of flash-induced FTIR defference spectra of the S-state cycle in the photosynthetic water-oxidizing complex by uniform ^{15}N and ^{13}C isotope labeling, *Biochemistry 42*, 6035−6042.
18. Yamanari, T., Kimura, Y., Mizusawa, N., Ishii, A., and Ono, T.-A. (2004) Mid- to low-frequency Fourier transform infrared spectra of S-state cycle for photosynthetic oxygen evolution in *Synechocystis* sp. PCC 6803, *Biochemistry 43*, 7479−7490.
19. Suzuki, H., Sugiura, M., and Noguchi, T. (2005) pH Dependence of the Flash-Induced S-State Transitions in the Oxygen-Evolving Center of Photosystem II from *Thermosynechococcus elongatus* as Revealed by Fourier Transform Infrared Spectroscopy, *Biochemistry 44*, 1708−1718.
20. Chu, H.-A., Sackett, H., and Babcock, G. T. (2000) Identification of a Mn−O−Mn cluster vibrational mode of the oxygen-evolving complex in photosystem II by low-frequency FTIR spectroscopy, *Biochemistry 39*, 14371−14376.
21. Chu, H.-A., Hillier, W., Law, N. A., and Babcock, G. T. (2001) Vibrational spectroscopy of the oxygen-evolving complex and of manganese model compounds, *Biochim. Biophys. Acta 1503*, 69−82.
22. Kimura, Y., Mizusawa, N., Ishii, A., Yamanari, T., and Ono, T.-A. (2003) Changes of low-frequency vibrational modes induced by universal ^{15}N- and ^{13}C-isotope labeling in S_2/S_1 FTIR difference spectrum of oxygen-evolving complex, *Biochemistry 42*, 13170−13177.
23. Cua, A., Stewart, D. H., Reifler, M. J., Brudvig, G. W., and Bocian, D. F. (2000) Low-frequency resonance Raman characterization of the oxygen-evolving complex of photosystem II, *J. Am. Chem. Soc. 122*, 2069−2077.
24. Schatz, G. H., and Witt, H. T. (1984) Extraction and characterization of oxygen-evolving photosystem II complexes from a thermophilic cyanobacterium *Synechococcus* spec., *Photobiochem. Photobiophys. 7*, 1−14.
25. Mühlenhoff, U., and Chauvat, F. (1996) Gene transfer and manipulation in the thermophilic cyanobacterium *Synechococcus elongatus*, *Mol. Gen. Genet. 252*, 93−100.
26. Mizusawa, N., Kimura, Y., Ishii, A., Yamanari, T., Nakazawa, S., Teramoto, H., and Ono, T.-A. (2004) Impact of replacement of D1 C-terminal alanine with glycine on structure and function of photosynthetic oxygen-evolving complex, *J. Biol. Chem. 279*, 29622−29627.
27. Chu, H.-A., Debus, R. J., and Babcock, G. T. (2001) D1-Asp170 is structurally coupled to the oxygen evolving complex in photosystem II as revealed by light-induced Fourier transform infrared difference spectroscopy, *Biochemistry 40*, 2312−2316.

28. Kimura, Y., Mizusawa, N., Yamanari, T., Ishii, A., and Ono, T.-A. (2005) Structural changes of D1 C-terminal α-carboxylate during S-state cycling in photosynthetic oxygen evolution, *J. Biol. Chem. 280*, 2078−2083.
29. Chu, H.-A., Hillier, W., Law, N. A., and Babcock, G. T. (2001) Identification of a possible Mn−O−Mn cluster vibrational mode of the S_3 state in the oxygen-evolving complex of photosystem II by low-frequency FTIR difference spectroscopy, *Proc. Int. Congr. Photosynth., 12th*, S13−027.
30. Cannon, R. D., Jayassooriya, U. A., Montri, L., Saad, A. K., Koru, E., Bollen, S. K., Sanderson, W. R., Powell, A. K., and Blake, A. B. (1993) Oxo-centered trinuclear carboxylato complexes containing mixed-metal and mixed-valence clusters $Cr^{III}_2M^{II}O$ and $Mn^{III}_2M^{II}O$ (M = Co, Ni or Mn), *J. Chem. Soc., Dalton Trans.*, 2005−2010.
31. Mrozek, R., Rzaczynska, Z., Sikorska-Iwan, M., Jaroniec, M., and Glowiak, T. (1999) A new complex of manganese(II) with l-α-alanine: structure, spectroscopy and thermal study, *Polyhedron 18*, 2321−2326.
32. Nakagawa, I., and Shimanouchi, T. (1964) Infrared absorption spectra of aquo complexes and the nature of co-ordination bonds, *Spectrochim. Acta 20*, 429−439.
33. Boucher, L. J., and Coe, C. G. (1975) Manganese-Schiff base complexes. VI. Synthesis and spectroscopy of aquo[*N*,*N*′-ethylenebis(4-*sec*-butylsalicylaldiminato)]manganese(III) perchlorate and μ-dioxo-bis[*N*,*N*′-ethylenebis(4-*sec*-butylsalicylaldiminato)]-dimanganese(IV) and the related *N*,*N*′-trimethylenebis(4-*sec*-butylsalicylaldimine) complexes, *Inorg. Chem. 14*, 1289−1295.
34. Cooper, S. R., and Calvin, M. (1977) Mixed valence interactions in di-μ-oxo bridged manganese complex, *J. Am. Chem. Soc. 99*, 6623−6630.
35. Dave, B. C., and Czernuszewicz, R. S. (1994) One-equivalent oxidative charge storage on an $[Mn_2O_2]^{3+}$ core: synthesis, crystal structure and resonance Raman spectra of $[Mn_2O_2(pbz)_4]^{n+}$ (n=3, 4), *Inorg. Chim. Acta 227*, 33−41.
36. Dave, B. C., and Czernuszewicz, R. S. (1998) Structural and spectroscopic models of the manganese catalase active site. Isolation and structures of the asymmetric $[(H_2O)Mn^{III}(\mu\text{-}O)\text{-}(\mu\text{-}O_2CR)_2Mn^{III}(L)]$ (L=$Cr_2O_7^{2-}$, CH_3OH) cores: analogs of a substrate-bound catalase active site intermediate, *Inorg. Chim. Acta 281*, 25−35.
37. Limburg, J., Vrettos, J. S., Chen, H., de Paula, J. C., Crabtree, R. H., and Brudvig, G. W. (2001) Characterization of the O_2-evolving reaction catalyzed by $[(terpy)(H_2O)Mn^{III}(O_2)Mn^{IV}(OH_2)(terpy)](NO_3)_3$ (terpy = 2,2′:6,2″-Terpyridine), *J. Am. Chem. Soc. 123*, 423−430.
38. Cua, A., Vrettos, J. S., de Paula, J. C., Brudvig, G. W., and Bocian, D. F. (2003) Raman spectra and normal coordinate analyses of low-frequency vibrations of oxo-bridged manganese complexes, *J. Biol. Inorg. Chem. 8*, 439−451.
39. Sheats, J. E., Czernuszewicz, R. S., Dismukes, G. C., Rheingold, A. L., Petrouleas, V., Stubbe, J., Armstrong, W. H., Beer, R. H., and Lippard, S. J. (1987) Binuclear manganese(III) complexes of potential biological significance, *J. Am. Chem. Soc. 109*, 1435−1444.
40. Johnson, M. K., Powell, D. B., and Cannon, R. D. (1981) Vibrational spectra of carboxylato complexes-III. Trinuclear 'basic' acetates and formats of chromium(III), iron(III) and other transition metals, *Spectrochim. Acta 37A*, 995−1006.
41. Meesuk, L., White, R. P., Templeton, B., Jayasooriya, U. A., and Cannon, R. D. (1990) Valence localization in triangular trimanganese(II, 2III) complexes, *Inorg. Chem. 29*, 2389−2392.
42. Messinger, J. (2004) Evaluation of different mechanistic proposals for water oxidation in photosynthesis on the basis of Mn_4O_xCa structures for the catalytic site and spectroscopic data, *Phys. Chem. Chem. Phys. 6*, 4764−4771.
43. Hillier, W., and Wydrzynski, T. (2004) Substrate water interactions within the photosystem II oxygen evolving complex, *Phys. Chem. Chem. Phys. 6*, 4882−4889.
44. Hoganson, C. W., and Babcock, G. T. (1997) A metalloradical mechanism for the generation of oxygen from water in photosynthesis, *Science 277*, 1953−1956.
45. Makino, R., Uno, T., Nishimura, Y., Iizuka, T., Tsuboi, M., and Ishimura, Y. (1986) Coordination structures and reactivities of compound II in iron and manganese horseradish peroxidases, *J. Biol. Chem. 261*, 8376−8382.
46. Czernuszewicz, R. S., Su, Y. O., Stern, M. K., Macor, K. A., Kim, D., Groves, J. T., and Spiro, T. G. (1988) Oxomanganese(IV) porphyrins identified by resonance Raman and infrared spectroscopy: weak bonds and the stability of the half-filled t_{2g} subshell, *J. Am. Chem. Soc. 110*, 4158−4165.
47. Groves, J. T., and Stern, M. K. (1988) Synthesis, characterization, and reactivity of oxomanganese(IV) porphyrin complexes, *J. Am. Chem. Soc. 110*, 8628−8638.
48. Nick, R. J., Ray, G. B., Fish, K. M., Spiro, T. G., and Groves, J. T. (1991) Evidence for a weak Mn═O bond and a non-porphyrin radical in manganese-substituted horseradish peroxidase compound I, *J. Am. Chem. Soc. 113*, 1838−1840.
49. Weng, T.-C., Hsieh, W.-Y., Uffelman, E. S., Gordon-Wylie, S. W., Collins, T. J., Pecoraro, V. L., and Penner-Hahn, J. E. (2004) XANES evidence against a manganyl species in the S_3 state of the oxygen-evolving complex, *J. Am. Chem. Soc. 126*, 8070−8071.
50. Hasegawa, K., Ono, T.-A., and Noguchi, T. (2000) Vibrational spectra and ab initio DFT calculations of 4-methylimidazole and its different protonation forms: Infrared and Raman markers of the protonation state of a histidine side chain, *J. Phys. Chem. B 104*, 4253−4265.
51. Socrates, G. (1994) in *Infrared and Raman Characteristic Group Frequencies*, 3rd ed., pp 333−335, John Wiley & Sons, Chichester, U.K.
52. Dau, H., Iuzzolino, L., and Dittmer, J. (2001) The tetra-manganese complex of photosystem II during its redox cycle—X-ray absorption results and mechanistic implications, *Biochim. Biophys. Acta 1503*, 24−39.
53. Schlodder, E., and Witt, H. T. (1999) Stoichiometry of proton release from the catalytic center in photosynthetic water oxidation, *J. Biol. Chem. 274*, 30387−30392.
54. Riggs-Gelasco, P. J., Mei, R., Ghanotakis, D. F., Yocum, C. F., and Penner-Hahn, J. E. (1996) X-ray absorption spectroscopy of calcium-substituted derivatives of the oxygen-evolving complex of photosystem II, *J. Am. Chem. Soc. 118*, 2400−2410.
55. Hendry, G., and Wydrzynski, T. (2002) The two substrate-water molecules are already bound to the oxygen-evolving complex in the S_2 state of photosystem II, *Biochemistry 41*, 13328−13334.
56. Visser, H., Dubé, C. E., Armstrong, W. H., Sauer, K., and Yachandra, V. K. (2002) FTIR spectra and normal-mode analysis of a tetranuclear manganese adamantane-like complex in two electrochemically prepared oxidation states: relevance to the oxygen-evolving complex of photosystem II, *J. Am. Chem. Soc. 124*, 11008−11017.
57. Robblee, J. H., Messinger, J., Cinco, R. M., McFarlane, K. L., Fernandez, C., Pizarro, S. A., Sauer, K., and Yachandra, V. K. (2002) The Mn cluster in the S_0 State of the oxygen-evolving complex of photosystem II studied by EXAFS spectroscopy: Are there three di-μ-oxo-bridged Mn_2 moieties in the tetranuclear Mn complex? *J. Am. Chem. Soc. 124*, 7459−7471.

BI048203D